

Accelerated Lanthanide Intercalation into Graphite Catalyzed by Na

Akira Iyo,^{1*} Hiroshi Fujihisa,¹ Yoshito Gotoh,¹ Shigeyuki Ishida,¹ Hiroshi Eisaki¹, Hiraku Ogino¹, Kenji Kawashima^{1,2}

¹National Institute of Advanced Industrial Science and Technology (AIST), Tsukuba, Ibaraki 305-8568, Japan

² IMRA JAPAN Co., Ltd., Kariya, Aichi 448-8650, Japan

KEYWORDS: Na catalyst, graphite intercalation compound, lanthanide-intercalated graphite (SmC₆, EuC₆, YbC₆), X-ray diffraction, resistivity, superconductivity

ABSTRACT: Lanthanides (*Ln*) are notoriously difficult to intercalate into graphite. We investigated the possibility of using Na to catalyze the formation of *Ln*-intercalated graphite and successfully synthesized *Ln*C₆ (*Ln* = Sm, Eu, and Yb) significantly rapidly in high yields. The synthesis process involves the formation of the reaction intermediate NaC_x, through the mixing of Na and C, which subsequently reacts with *Ln* upon heating to form *Ln*C₆. Well-sintered *Ln*C₆ pellets with low residual Na concentrations (*Ln*:Na ≈ 98:2) were fabricated by the two-step method. The pellets enabled the evaluation of *Ln*C₆ by powder X-ray diffraction and electrical resistivity measurements. This study highlights the versatility of the Na-catalyzed method and lays the foundation for the rapid mass production of *Ln*C₆, with potential applications in superconducting and rechargeable battery materials.

1. INTRODUCTION

Graphite intercalation compounds (GICs) are formed by the insertion of atoms or molecules (intercalates) into graphite, consisting of stacks of graphene sheets. Alkali metals (*A_M*), alkaline earth metals (*A_E*), and lanthanoids (*Ln*) are known as typical donor-type intercalates. Among these,

A_M can easily intercalate into the graphite, allowing for the synthesis of A_M -GIC bulk samples by the vapor-phase method.¹ In contrast, the intercalation of A_E or Ln is not as facile. Bulk samples of A_E -GICs (A_EC_6) have been synthesized by the molten alloy^{2,3} and molten salt^{4,5} methods. However, these methods commonly require time-consuming heat treatment at a temperature (T) of 350 °C for approximately a week.

Recently, the use of Na as a catalyst was reported to drastically accelerate the formation of an A_E -GIC (A_EC_6).^{6,7} Bulk samples of A_EC_6 can be produced by simply mixing A_E and C powders with Na at room temperature, followed by heat treatment at a relatively low T (250 °C) for just a few hours. This Na-catalyzed method is characterized by the formation of the reaction intermediate NaC_x (stage 6–8 Na-GIC with x of 48–64)^{8,9} via the mixing of Na with C. Owing to its instability,^{10,11} NaC_x transforms to the more stable A_EC_6 by reacting with A_E upon heating.

The intercalation of lanthanides (Ln) into graphite is even more challenging. In 1980, Makrini et al. attempted the synthesis of Ln -GICs (LnC_6) for $Ln = Sm, Eu, Tm, \text{ and } Yb$.¹² However, even with an extended period of heat treatment (≈ 20 d), the yield reached a maximum of only 25% for EuC_6 . Hagiwara et al. reported the formation of LnC_6 ($Ln = Nd, Sm, Dy, Er, \text{ and } Yb$) by immersing highly oriented pyrolytic graphite (HOPG) in a eutectic molten solution of LiCl-KCl containing Ln and $LnCl_3$, followed by 4–5 days of heat treatment.¹³ However, their paper only presented the lattice constants, and lacked descriptions of the X-ray diffraction (XRD) patterns and yields of LnC_6 . Despite subsequent attempts to synthesize YbC_6 using either the vapor-phase^{14,15} or the molten salt¹⁶ method, YbC_6 was limited to forming on the surface of HOPG. Only EuC_6 was synthesized in the bulk form via heat treatment at 350 °C for 10 days using either the molten salt¹⁷ or the molten alloy¹⁸ method.

The above-mentioned unsatisfactory yields and time-consuming processes have limited the research and development of LnC_6 for potential applications such as superconducting materials,¹⁴ hydrogen storage materials,¹⁹ and anode materials for secondary batteries.^{20,21} This motivated us to devise a more efficient method for the synthesis of bulk quantities of LnC_6 by applying the Na-catalyzed method. Initially, the potential for Na-catalyzed Ln -GIC formation was comprehensively investigated for $Ln = La, Ce, Pr, Nd, Sm, Eu, Gd, Tb, Dy, Ho, Er, Tm, Yb, \text{ and } Lu$. As a result, the three LnC_6 ($Ln = Sm, Eu, \text{ and } Yb$) were found to form significantly rapidly in high yields although the catalytic effect of Na did not lead to the formation of Ln -GICs that had not been synthesized previously. In this paper, we report the details of the Na-catalyzed synthesis of LnC_6 ($Ln = Sm,$

Eu, and Yb) and an experimental study on their formation process. Furthermore, we fabricated LnC_6 pellets with low residual Na concentrations and evaluated their physical properties via powder XRD and electrical resistivity measurements. This paper provides a foundation for the efficient production of LnC_6 and encourages the research and development of LnC_6 for various applications.

2. EXPERIMENTAL SECTION

2.1 Sample Preparation

Graphite powder (Furuuchi Chemical Corp., 99.99%, -200 mesh) was employed as the host for intercalation. Ln lumps (Furuuchi Chemical, 99.5%) were filed down to powder form prior to use. The soft metal Na was used by directly cutting off a lump (Furuuchi Chemical, 99.9%). In a previous study,^{6,7} the materials of Na, A_E , and C were mixed simultaneously. In this study, Ln powder and Na were first mixed (kneaded) for ~ 15 min using a mortar and pestle to finely disperse the Ln particles in Na. C powder was then added to this mixture of Ln and Na (the materials weighed ~ 0.2 g in total), whereupon mixing was continued for an additional 15 min. We used a mixing ratio of $Ln:C:Na = 1:6:2$, where the mixing ratio of Na was determined in another study that synthesized CaC_6 under conditions similar to those of this study.⁷ The resulting sample was pressed into a pellet. The pellet was sealed in either stainless steel (SST) or quartz tubes. Owing to the reactivity of Na with quartz, SST tubes were preferentially used for heating above 275 °C for more than 2 h. The detailed heat-treatment conditions of the samples are described in the following sections. As the Ln , Na and LnC_6 samples are unstable in air, they were handled in an Ar-filled glove box.

2.2 Measurements

XRD experiments were conducted using $CuK\alpha$ radiation on a Rigaku Ultima IV instrument with an airtight attachment to prevent the sample from being exposed to air. Samples without Na reduction could not be powdered owing to their high viscosity, which inevitably led to the c -axis orientation of LnC_6 crystals at the sample surface when they were placed on the sample plate for XRD measurements. In contrast, samples from which most of the Na had been removed could be powdered, enabling the collection of XRD patterns with a suppressed orientation.

The compositions of the samples were analyzed using an energy-dispersive X-ray spectrometer (Oxford, SwiftED3000) equipped with an electron microscope (Hitachi High Technologies, TM-3000). The dependence on T of the resistivity (ρ) was measured utilizing the four-terminal method on a physical property measuring system (Quantum Design, PPMS). The electrodes were affixed to the sample in a glove box using Ag paste (DuPont 4922N). Once the Ag paste had dried, the sample was covered with Apiezon N grease to prevent exposure to air. The dependence of the magnetization (M) on T was measured using a magnetic property measurement system (Quantum Design, PPMS).

3. RESULTS AND DISCUSSION

3.1 Control experiments to Verify Catalytic Effect of Na

Prior to the Na-catalyzed synthesis of LnC_6 , control experiments were conducted to determine the extent to which LnC_6 ($Ln = Sm, Eu, \text{ and } Yb$) forms without the addition of Na. Ln and C powders were mixed in a molar ratio $Ln:C$ of 1:6, pelletized, and heat-treated at 275 °C for 6 h in SST tubes. The powder XRD patterns of the resulting samples are shown in Figure 1. For $Ln = Eu$, although clear diffraction peaks from EuC_6 were observed, the majority of the sample still consisted of unreacted Eu and C. For $Ln = Yb$, only tiny diffraction peaks from YbC_6 were detected, and SmC_6 , known for its challenging synthesis as mentioned in the literature,¹² did not form at all.

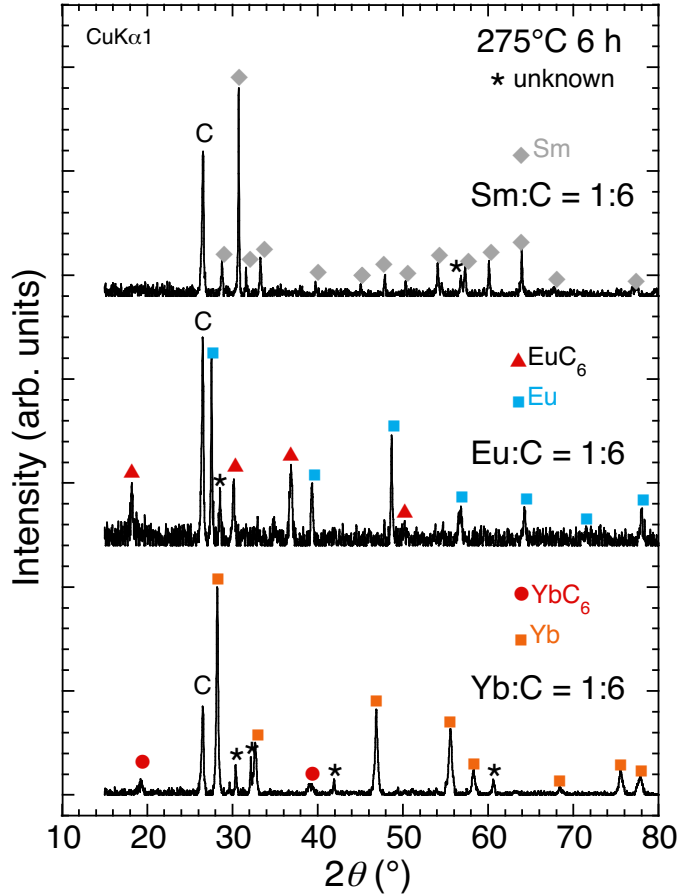


Figure 1. Powder XRD patterns of samples prepared without the addition of Na. The experiments were performed as a control to examine the catalytic effect of Na on the formation of LnC_6 ($Ln = \text{Sm}, \text{Eu}, \text{and Yb}$).

Next, we investigated the catalytic effect of Na on the formation of SmC_6 as a function of the heat-treatment temperature (T_h). Samples with a Sm:C:Na mixing ratio of 1:6:2 were pelletized and sealed in quartz tubes, followed by heat treatment at T_h of 150, 225, and 275 °C for 2 h. The XRD patterns of the samples are presented in Figure 2 as a function of T_h . In the as-mixed sample (i.e., without heat treatment), only NaC_x was formed by the reaction of C and Na, whereas Sm remained unreacted. The formation of NaC_x by mixing alone has also been observed in the synthesis of Li-GIC and CaC_6 .^{6,7} At $T_h = 150$ °C, SmC_6 did not form, and instead, an unknown phase (presumed to be a Na-Sm binary compound) was generated as denoted by asterisks. At $T_h = 225$ °C, the emergence of the diffraction peaks confirmed the formation of SmC_6 . However, the sample still contained a significant fraction of the unreacted Sm and the unknown phase. At $T_h = 275$ °C, the yield of SmC_6 increased rapidly, accompanied by a marked decrease in the peak

intensities of the unknown phase and NaC_x . These results, compared to the results of the control experiment, clearly demonstrate that Na has a strong catalytic effect on the formation of SmC_6 , with NaC_x acting as a reaction intermediate of the catalyst.

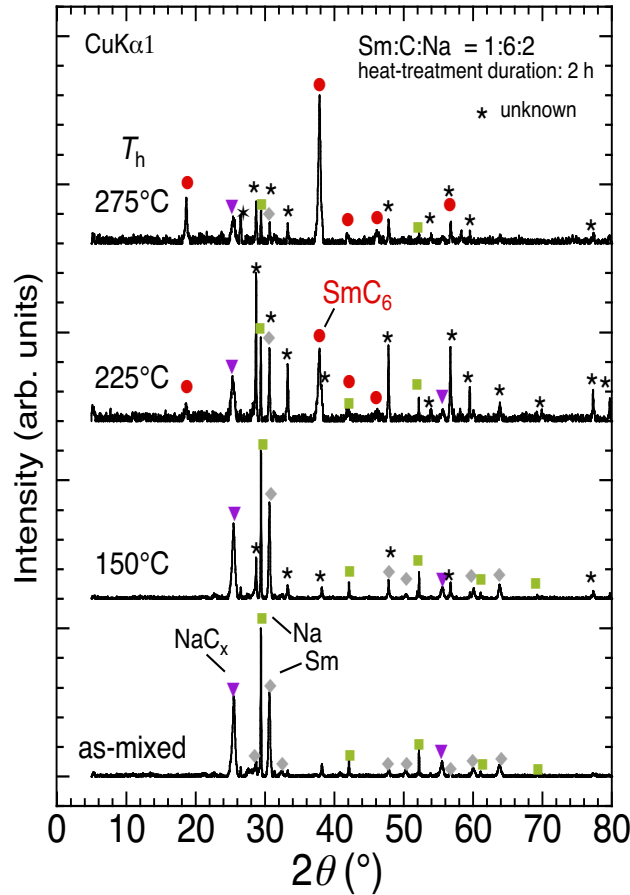


Figure 2. XRD patterns of samples ($\text{Sm:C:Na} = 1:6:2$) as a function of the heat-treatment temperature (T_h).

Next, we investigated the catalytic effect of Na as a function of the heat-treatment duration (D_h) for YbC_6 . Samples with a Yb:C:Na mixing ratio of 1:6:2 were pelletized and placed in SST tubes, followed by heat treatment at 275 °C for D_h of 0.25, 1, and 6 h. The acquired XRD patterns are shown in Figure 3. The XRD pattern of the as-mixed sample, shown by the dashed curve, primarily consisted of the diffraction peaks of NaC_x , Yb, and Na. With a heat treatment of only $D_h = 0.25$ h, a high-intensity diffraction peak of YbC_6 appeared at $2\theta \approx 39^\circ$, accompanied by a significant decrease in the intensity of the NaC_x and Yb peaks. This is clearly indicative of the formation of

YbC_6 via the reaction between NaC_x and Yb. By increasing D_h to 1 h and then 6 h, the formation of YbC_6 progressed steadily. Thus, the catalytic effect of Na drastically accelerated the formation of LnC_6 .

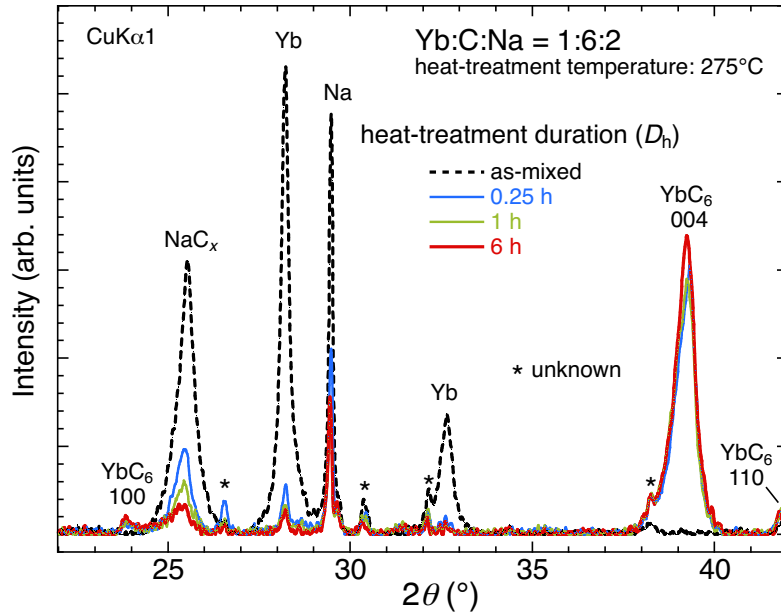


Figure 3. XRD patterns of the samples ($\text{Yb:C:Na} = 1:6:2$) as a function of the heat-treatment duration (D_h).

3.2 Fabrication of Pellets with Reduced Residual Na

Samples prepared by the Na-catalyzed method inevitably result in the mixture of LnC_6 and Na. For the potential application of LnC_6 , the residual Na in the sample needs to be minimized. Samples with a Ln:C:Na mixing ratio of 1:6:2 ($\text{Ln} = \text{Sm}, \text{Eu}, \text{and Yb}$) were pressed into pellets (the weight of each pellet was approximately 200 mg). The samples were heated at 275 °C in SST tubes for a total duration of 12 h for $\text{Ln} = \text{Sm}$ and Yb, and 4 h for $\text{Ln} = \text{Eu}$. The heat treatment was interrupted once for an intermediate mixing of the sample to improve the yield and homogeneity of LnC_6 .

Subsequently, using a two-step Na reduction process,⁷ polycrystalline pellets with low residual Na concentrations were fabricated. The Ln:Na composition ratio of the pellets was measured to be $\approx 98:2$. Because the intercalated Ln is divalent, as is the case for A_E ,²² the LnC_6 pellets have a light golden color similar to that of A_EC_6 ,⁶ as shown in Figure 4. The densities of the LnC_6 pellets ($\text{Ln} = \text{Sm}, \text{Eu}, \text{and Yb}$) were 3.66, 3.69, and 4.29 g/cm^3 , respectively, approximately 77% of the

theoretical density. Note that this is the first time that bulk samples of SmC_6 and YbC_6 were successfully fabricated.



Figure 4. Polycrystalline LnC_6 pellets ($\text{Ln} = \text{Sm}, \text{Eu}, \text{and Yb}$) with low residual Na concentrations ($\text{Ln}:\text{Na} \approx 98:2$).

The XRD patterns of the LnC_6 powders ($\text{Ln} = \text{Sm}, \text{Eu}, \text{and Yb}$) acquired by grinding the pellets are depicted in Figure 5a. By carefully placing the powders on the sample plates to minimize the preferred orientation of LnC_6 crystals, XRD patterns containing peaks with diffraction indices other than $00l$ were obtained.

The diffraction peaks of LnC_6 ($\text{Ln} = \text{Sm}$ and Eu) could be indexed well by assuming the same hexagonal system ($P6_3/mmc$) as BaC_6 and SrC_6 . The appearance of $h00$ diffraction peaks is a hallmark of the hexagonal crystal system. The diffraction peaks of YbC_6 could also be indexed basically by assuming the same hexagonal system. However, the $00l$ diffraction peaks were broad, and weak diffraction components that could be explained by assuming a rhombohedral crystal system ($R-3m$) appeared (denoted by arrows). This suggests that the rhombohedral stacking sequence of Yb and graphene layers ($A\alpha A\beta A\gamma A\alpha$) coexisted with the hexagonal stacking sequence ($A\alpha A\beta A\alpha A\beta$).¹² Note that CaC_6 , synthesized via the Na-catalyzed method, is suggested to have an inverse stacking sequence disorder ($A\alpha A\beta A\gamma A\alpha$ stacking sequence combined with $A\alpha A\beta A\alpha A\beta$).⁷

Table 1 presents the a - and c -axis lengths of unit cells, interlayer distances (d_s), and unit cell volumes (V) of LnC_6 derived from the analysis of the powder XRD patterns. The interlayer distance refers to the spacing between adjacent graphene layers, corresponding to half the c -axis length for LnC_6 . Our values are in close agreement with those in the literature.¹² The d_s values of LnC_6 and A_EC_6 obtained by the Na-catalyzed method are plotted against the ionic radii of divalent lanthanides (Ln^{2+}) and alkaline earth metals (A_E^{2+}) in Figure 5b.²³ The relationship between the ionic radii and d_s is approximately linear. Despite the close proximity of YbC_6 and CaC_6 , the

structural boundary between rhombohedral and hexagonal systems exists between them. Therefore, it seems natural for two different stacking sequences to intermingle in YbC_6 and CaC_6 as a result of the Na-catalyzed rapid synthesis.

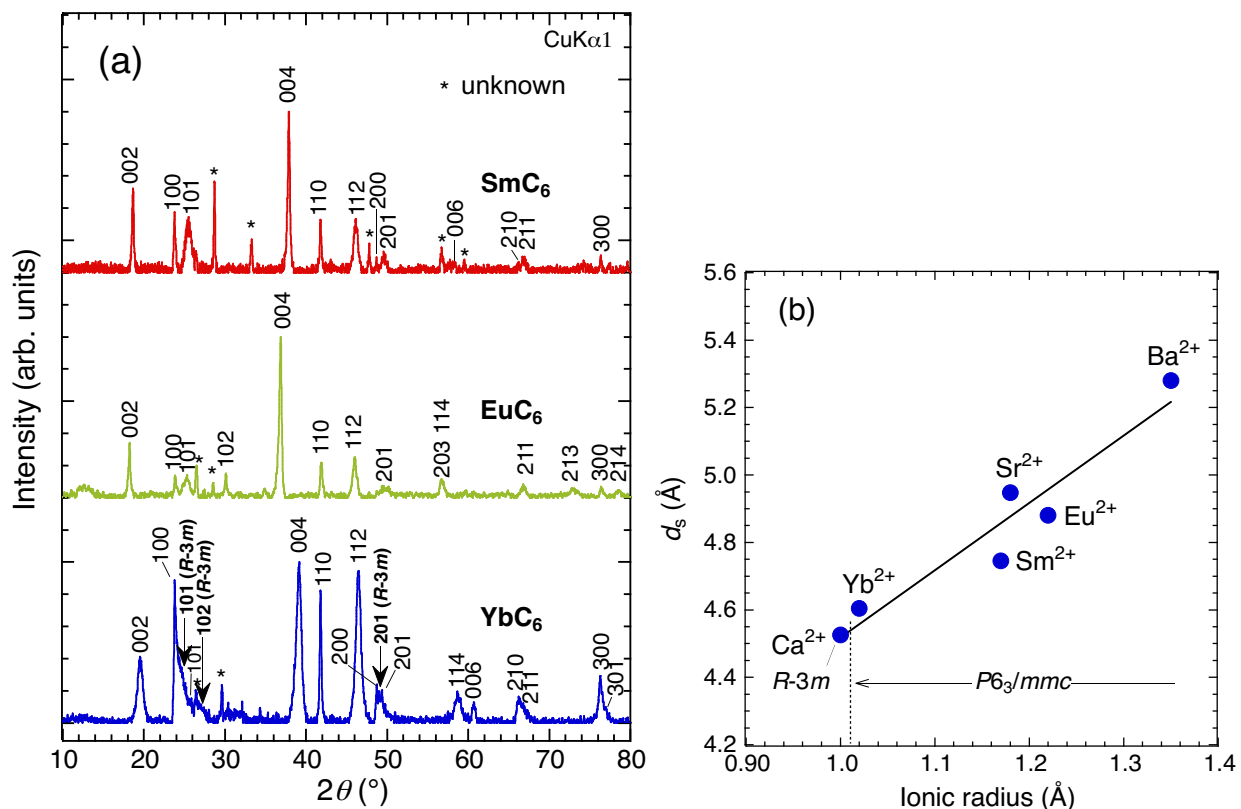


Figure 5. (a) Powder XRD patterns of LnC_6 ($\text{Ln} = \text{Sm}, \text{Eu}, \text{and Yb}$). The diffraction peaks are indexed assuming a hexagonal crystal system ($P6_3/mmc$). For YbC_6 , the diffraction angles and indices (hexagonal setting) that appear when the rhombohedral crystal system ($R-3m$) is assumed are also indicated. (b) Correlation between the interlayer distance (d_s) and the ionic radius of divalent Ln and A_E for LnC_6 and A_EC_6 .

Table 1. a - and c -axis lengths of unit cells, interlayer distances (d_s), and unit cell volumes (V) of LnC_6 synthesized in this study, along with values reported in the literature.¹²

GICs	a (Å)	c (Å)	d_s (Å)	V (Å ³)	Refs.
SmC ₆	4.319(1)	9.490(2)	4.745(1)	153.3(1)	this study
	–	~9.40	~4.70	–	12
EuC ₆	4.319(1)	9.761(1)	4.881(1)	157.7(1)	this study
	4.314(3)	9.745(8)	4.873(4)	157.2	12
YbC ₆	4.320(1)	9.207(1)	4.604(1)	148.8(1)	this study
	4.320(4)	9.147(4)	4.574(2)	147.8	12

3.3 Physical Properties of LnC_6

The low residual Na concentration in the LnC_6 pellets minimizes the effect of Na on transport properties. The dependence of the resistivity ρ on T for LnC_6 ($Ln = \text{Sm}, \text{Eu}, \text{and Yb}$) is depicted in Figure 6a. All samples exhibit metallic behavior, with ρ in the range of 0.3–0.4 mΩ cm at 300 K; however, their behaviors diverge at lower T . While SmC₆ did not exhibit anomalous behavior above 2 K, a bump corresponding to a magnetic phase transition was detected at 39.0 K in EuC₆.^{22,24}

For YbC₆, an abrupt resistive drop due to the occurrence of superconductivity was observed at a midpoint (onset) transition temperature of $T_c^{\text{mid}} = 5.1$ K ($T_c^{\text{onset}} = 6.0$ K), as indicated in the inset. The superconductivity was also confirmed by magnetization measurements (Figure 6b). The nearly 100% shielding volume fraction ($4\pi M/H \approx -1$ at 2 K in the zero-field-cooling (ZFC) curve) indicates that the sample is well-sintered. The YbC₆ sample prepared in this study exhibited a lower superconducting transition temperature by ~ 1 K than YbC₆ samples prepared by vapor-phase methods ($T_c = 6.5$ K),^{14,15} possibly due to the stacking sequence disorder.

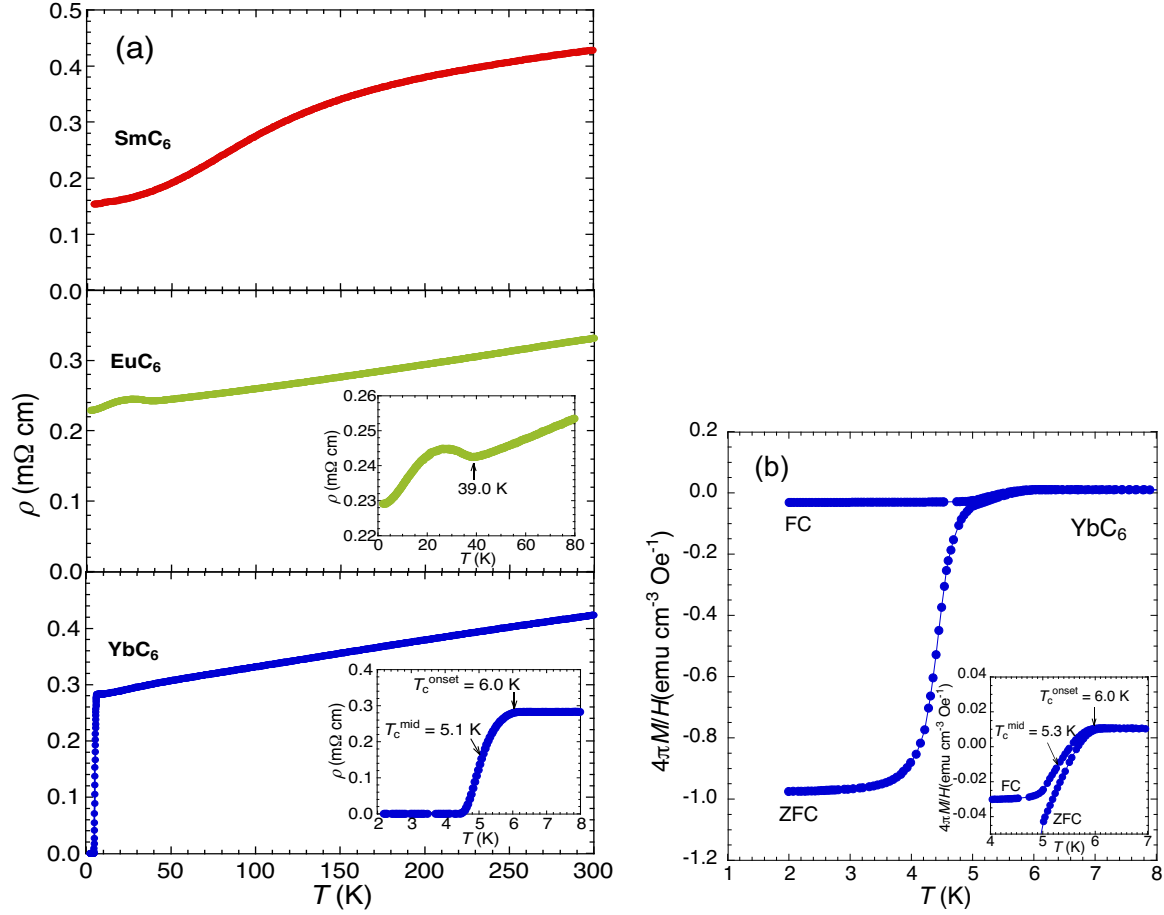


Figure 6. (a) T dependence of ρ for polycrystalline LnC_6 ($\text{Ln} = \text{Sm}, \text{Eu}, \text{and Yb}$) in the range of 2–300 K. The inset provides an enlarged view near the magnetic and superconducting transitions. T_c^{mid} is defined as the T where ρ decreases to half of the value in the normal state just above T_c . (b) T dependence of M for YbC_6 in the range of 2–8 K. M was measured in the zero-field-cooling (ZFC) and field-cooling (FC) modes in a magnetic field (H) of 10 Oe. M was corrected by the demagnetization coefficient based on the sample geometry. The inset shows an enlarged view near T_c .

Figure 7a shows the shift of the resistive superconducting transition by applying H of up to 14 kOe. The nearly parallel transition shift indicates the good sintering and homogeneity of the pellet. Figure 7b presents the dependence of the upper critical field (H_{c2}) on T , defined at T_c^{onset} , T_c^{mid} , and T_c^{end} as marked by arrows in the figure, along with previously reported data for YbC_6 .^{14,15}

For all YbC_6 shown in Figure 7b, H_{c2} increased linearly with lowering T , a common feature also observed in CaC_6 .^{7,25} However, the H_{c2} in this study was enhanced by a factor of 3–5 over previously reported values for YbC_6 slowly synthesized by the vapor-phase method. Extrapolating

H_{c2} defined at T_c^{mid} to 0 K yields $H_{c2}(0) = 16.0$ kOe, as indicated in Figure 7a. The coherence length $\xi_{\text{GL}}(0)$ is derived to be 143 Å from the Ginzburg-Landau formula $H_{c2} = \Phi_0/(2\pi\xi_{\text{GL}}^2)$, where Φ_0 is the flux quantum. The $\xi_{\text{GL}}(0)$ is much shorter than previously reported values of 170–450 Å.^{14,15,26} The stacking sequence disorder suggested by the powder XRD analysis is possibly responsible for the short $\xi_{\text{GL}}(0)$, resulting in the enhanced H_{c2} . A similar trend was observed for CaC₆ synthesized using the Na-catalyzed method⁷; however, it was more pronounced for YbC₆.

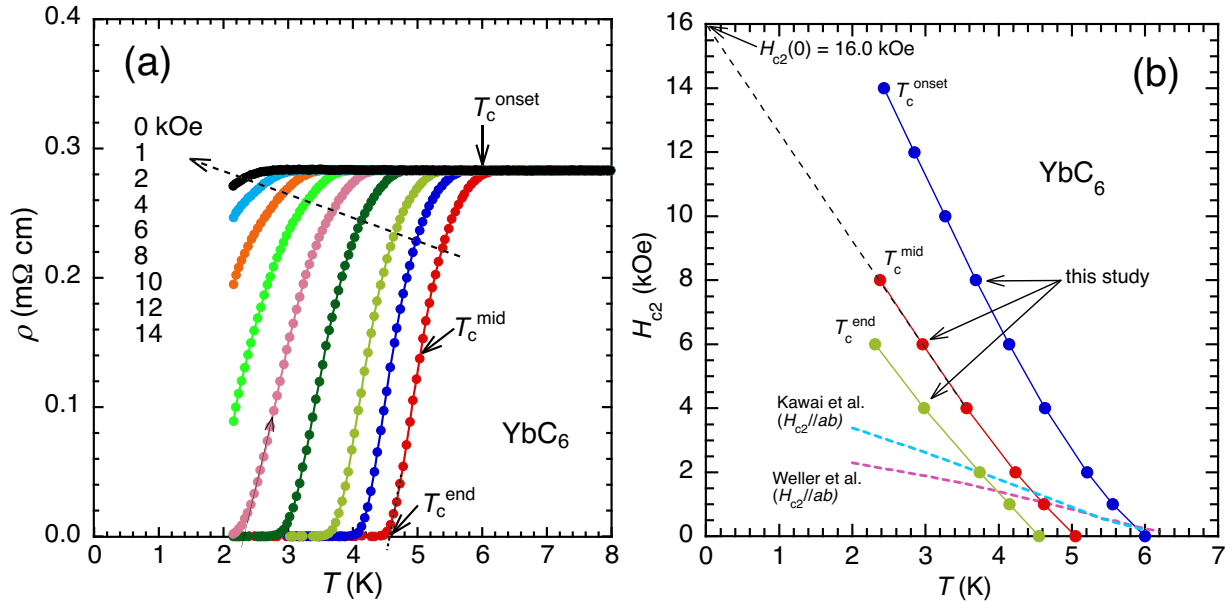


Figure 7. (a) Superconducting resistive transition shift in YbC₆ in a magnetic field from 0 to 14 kOe. The pellet is *c*-axis-oriented perpendicular to its plane, and *H* is applied to a rectangular sample cut from the pellet such that it is parallel to the *ab* plane (*H*//*ab*). (b) Dependence of H_{c2} on T , defined at T_c^{onset} , T_c^{mid} , and T_c^{end} , along with previously reported data. The dashed line represents the linear extrapolation of H_{c2} defined at T_c^{mid} .

4. CONCLUSIONS

The Na-catalyzed method was demonstrated to be highly effective for the synthesis of LnC_6 ($Ln = \text{Sm}, \text{Eu}, \text{and Yb}$). In particular, SmC₆ and YbC₆, which proved to be difficult to synthesize without the addition of Na, were rapidly formed in the presence of Na. Systematic synthesis experiments clearly captured the process by which the reaction intermediate NaC_{*x*} reacted with *Ln* to form SmC₆ and YbC₆. Well-sintered pellets with reduced catalytic Na concentrations ($Ln:Na \approx 98:2$) were shown to be feasible. YbC₆, located at the structural phase boundary, exhibited stacking

sequence disorder because of its rapid formation catalyzed by Na, which is a possible cause of the large H_{c2} enhancement. The Na-catalyzed method has versatility and is expected to be applied to more diverse intercalates in the future. Thus, this study lays the foundation for the rapid mass production of LnC_6 . The development of a more practical synthesis method for LnC_6 , along with an assessment of its potential applications, is a direction for future work.

AUTHOR INFORMATION

Corresponding Author

Akira Iyo, E-mail: iyo-akira@aist.go.jp

The manuscript was written through the contributions of all authors. All authors have approved the final version of the manuscript.

Funding Sources

The Japan Society for the Promotion of Science (JSPS) Grants-in-Aid for Scientific Research (KAKENHI) (22K04193).

Notes

The authors declare no competing financial interest.

Data Availability Statement

The data supporting the findings of this study are available from the corresponding author upon reasonable request.

ACKNOWLEDGMENT

This study was partly supported by the Japan Society for the Promotion of Science (JSPS) Grants-in-Aid for Scientific Research (KAKENHI) (22K04193).

REFERENCES

- (1) Dresselhaus, M. S.; Dresselhaus, G. Intercalation Compounds of Graphite. *Adv. Phys.* **1981**, *30*, 139. <https://doi.org/10.1080/00018738100101367>.
- (2) Emery, N.; Hérold, C.; Lagrange, P. The Synthesis of Binary Graphite-Metal Intercalation Compounds Using Molten Lithium Alloys. *Carbon* **2008**, *46* (1), 72-75. <https://doi.org/10.1016/j.carbon.2007.10.039>.
- (3) Emery, N.; Hérold, C.; Lagrange, P. Overview on the Intercalation Reactions of Lithium Alloys into Graphite. *Prog. Solid State Chem.* **2008**, *36* (3), 213-222. <https://doi.org/10.1016/j.progsolidstchem.2008.07.002>.
- (4) Fauchard, M.; Cahen, S.; Bolmont, M.; Medjahdi, G.; Lagrange, P.; Hérold, C. An Efficient Medium to Intercalate Metals into Graphite: LiCl-KCl Molten Salts. *Carbon* **2019**, *144*, 171. <https://doi.org/10.1016/j.carbon.2018.12.014>.
- (5) El Hajj, I.; Speyer, L.; Cahen, S.; Herbuvaux, L.; Lagrange, P.; Medjahdi, G.; Hérold, C. Intercalation of Barium into Graphite by Molten Salts Method: Synthesis of Massive Samples for Crystal Structure Determination of BaC₆. *Carbon* **2022**, *186*, 431-436. <https://doi.org/10.1016/j.carbon.2021.09.073>.
- (6) Iyo, A.; Ogino, H.; Ishida, S.; Eisaki, H. Dramatically Accelerated Formation of Graphite Intercalation Compounds Catalyzed by Sodium. *Adv. Mater.* **2023**, *35* (28), 2209964. <https://doi.org/10.1002/adma.202209964>.
- (7) Iyo, A.; Fujihisa, H.; Gotoh, Y.; Ishida, S.; Eisaki, H.; Ogino, H.; Kawashima, K. Na-Catalyzed Rapid Synthesis and Characterization of Intercalated Graphite CaC₆. *Carbon* **2023**, *215*, 118381. <https://doi.org/10.1016/j.carbon.2023.118381>.
- (8) Asher, R. C. A Lamellar Compound of Sodium and Graphite. *J. Inorg. Nucl. Chem.* **1959**, *10*, 238-249. [https://doi.org/10.1016/0022-1902\(59\)80118-4](https://doi.org/10.1016/0022-1902(59)80118-4).
- (9) Metrot, A.; Guerard, D.; Billaud, D.; Hérold, A. New results about the sodium-graphite system. *Synth. Met.* **1980**, *1*, 363-369. [https://doi.org/10.1016/0379-6779\(80\)90071-5](https://doi.org/10.1016/0379-6779(80)90071-5).

- (10) Moriwake, H.; Kuwabara, A.; Fisher, C. A.; Ikuhara, Y. Why Is Sodium-Intercalated Graphite Unstable? *RSC Adv.* **2017**, *7* (64), 36550. <https://doi.org/10.1039/c7ra06777a>.
- (11) Lenchuk, O.; Adelhelm, P.; Mollenhauer, D. New Insights into the Origin of Unstable Sodium Graphite Intercalation Compounds. *Phys. Chem. Chem. Phys.* **2019**, *21* (35), 19378. <https://doi.org/10.1039/c9cp03453f>.
- (12) Makrini, M. E.; Guérard, D.; Lagrange, P.; Hérold, A. Intercalation of Rare Earth Metals in Graphite. *Physica B+C* **1980**, *99*, 481-485. [https://doi.org/10.1016/0378-4363\(80\)90282-X](https://doi.org/10.1016/0378-4363(80)90282-X).
- (13) Hagiwara, R.; Ito, M.; Ito, Y. Graphite Intercalation Compounds of Lanthanides Metals Prepared in Molten Chlorides. *Carbon* **1996**, *34* (12), 1591-1593. [https://doi.org/10.1016/S0008-6223\(96\)00109-1](https://doi.org/10.1016/S0008-6223(96)00109-1).
- (14) Weller, T.; Ellerby, M.; Saxena, S.; Smith, R. P.; Skipper, N. T. Superconductivity in the Intercalated Graphite Compounds C_6Yb and C_6Ca . *Nat. Phys.* **2005**, *1*, 39. <https://doi.org/10.1038/nphys0010>.
- (15) Kawai, N. F.; Fukuyama, H. Anisotropic Superconductivity in Graphite Intercalation Compound YbC_6 . *Physica C* **2008**, *468*, 2403-2407. <https://doi.org/10.1016/j.physc.2008.09.009>.
- (16) Cahen, S.; El-Hajj, I.; Speyer, L.; Berger, P.; Medjahdi, G.; Lagrange, P.; Lamura, G.; Hérold, C. Original Synthesis Route of Bulk Binary Superconducting Graphite Intercalation Compounds with Strontium, Barium and Ytterbium. *New J. Chem.* **2020**, *44* (24), 10050. <https://doi.org/10.1039/c9nj06423k>.
- (17) Bolmont, M.; Cahen, S.; Fauchard, M.; Guillot, R.; Medjahdi, G.; Berger, P.; Lamura, G.; Lagrange, P.; Hérold, C. LiCl-KCl Eutectic Molten Salt as an Original and Efficient Medium to Intercalate Metals into Graphite: Case of Europium. *Carbon* **2018**, *133*, 379-383. <https://doi.org/10.1016/j.carbon.2018.03.015>.
- (18) Rida, H.; Cahen, S.; Hérold, C.; Lagrange, P. Bulk Synthesis and Crystal Structure of the First Stage Europium–Graphite Intercalation Compound. *Carbon* **2010**, *48* (12), 3190-3195. <https://doi.org/10.1016/j.carbon.2010.04.056>.

- (19) Gadipelli, S.; Guo, Z. X. Graphene-Based Materials: Synthesis and Gas Sorption, Storage and Separation. *Prog. Mater. Sci.* **2015**, *69*, 1-60. <https://doi.org/10.1016/j.pmatsci.2014.10.004>.
- (20) Enoki, T.; Suzuki, M.; Endo, M. Graphite Intercalation Compounds and Applications; Oxford University Press: London, **2003**.
- (21) Xu, J.; Dou, Y.; Wei, Z.; Ma, J. N.; Deng, Y.; Li, Y.; Liu, H.; Dou, S. Recent Progress in Graphite Intercalation Compounds for Rechargeable Metal (Li, Na, K, Al)-Ion Batteries. *Adv. Sci.* **2017**, *4*, 1700146. <https://doi.org/10.1002/advs.201700146>.
- (22) Suematsu, H.; Ohmatsu, K.; Sakakibara, T.; Date, M.; Suzuki, M. Magnetic Properties of Europium-Graphite Intercalation Compound C₆Eu. *Synth. Met.* **1983**, *8*, 23-30. [https://doi.org/10.1016/0379-6779\(83\)90005-X](https://doi.org/10.1016/0379-6779(83)90005-X).
- (23) Shannon, R. D. Revised Effective Ionic Radii and Systematic Studies of Interatomic Distances in Halides and Chalcogenides. *Acta Cryst. A* **1976**, *32*, 751–767. <https://doi.org/10.1107/S056773947600155>.
- (24) Chen, S. T.; Dresselhaus, M. S.; Dresselhaus, G.; Suematsu, H.; Minemoto, H.; Ohmatsu, K.; Yosida, Y. Magnetoresistivity and Monte Carlo Studies of Magnetic Phase Transitions in C₆Eu. *Phys. Rev. B* **1986**, *34*, 423–430. <https://doi.org/10.1103/physrevb.34.423>.
- (25) Jobiliong, E.; Zhou, H. D.; Janik, J. A.; Jo, Y.-J.; Balicas, L.; Brooks, J. S.; Wiebe, C. R. Anisotropic Superconductivity in Bulk CaC₆. *Phys. Rev. B* **2007**, *76*, 052511. <https://doi.org/10.1103/PhysRevB.76.052511>.
- (26) Smith, R. P.; Weller, T. E.; Howard, C. A.; Dean, M. P. M.; Rahnejat, K. C.; Saxena, S. S.; Ellerby, M. Superconductivity in Graphite Intercalation Compounds, *Physica C* **2015**, *514*, 50-58, <https://doi.org/10.1016/j.physc.2015.02.029>.